

Structure and dynamics of alkali-metal clusters and fission of highly charged clusters

Yibing Li and Estela Blaisten-Barojas*

Institute for Computational Sciences and Informatics, George Mason University, Fairfax, Virginia 22030

D. A. Papaconstantopoulos

Institute for Computational Sciences and Informatics, George Mason University, Fairfax, Virginia 22030

and Complex Systems Theory Branch, Naval Research Laboratory, Washington, D.C. 20375-5320

(Received 13 May 1997; revised manuscript received 19 December 1997)

A dynamical optimization of the minimum energy cluster structures of Na, K, Rb, and Cs clusters was performed using a many-body potential based on local density calculations. The energetics and vibrational analysis of the neutral clusters in the size range $8 < N < 310$ were calculated, including the free energy as a function of the cluster size and the melting temperature. The fission process due to Coulomb forces of $2+$, $3+$, and $4+$ charged alkali-metal clusters was studied extensively using molecular dynamics. We show that the cluster size at which multiply charged clusters undergo fission depends strongly on the cluster temperature. Three phases in the temperature-size-phase plane are identified corresponding to unstable, metastable, and stable clusters. These regions are bound by the spontaneous size at zero temperature and the critical size at the critical temperature. The cluster critical size exhibits a power law dependence on the total charge, which is in excellent agreement with experiments. The energy barriers that the clusters need to undergo fission are reported as a function of cluster size. The limitations of the liquid drop model are indicated in light of the dynamical findings. [S0163-1829(98)05624-0]

I. INTRODUCTION

Considerable experimental¹⁻¹⁰ and theoretical¹¹⁻¹⁵ effort has taken place in recent years to study the fission of multiply charged alkali-metal clusters. The study of charged clusters is of fundamental importance since cluster detection through mass spectrometry proceeds via ionization and detection of charged species. Singly ionized clusters of most elements are stable at low temperature while multiply charged clusters are not, because the Coulomb repulsion between the charges acts against the cohesive forces. Fission of multiply ionized clusters presents strong analogies to corresponding phenomena exhibited by heavy atomic nuclei. Experimental fission patterns (symmetric versus asymmetric fission) and fission barriers have been interpreted^{2-4,6-9,11,16} within the framework of the liquid-droplet model of nuclear theory.¹⁷ In those models, only the initial and final state energies are taken into account. Predictions exist of fragmentation channels of $2+$ cluster ions using the local density approximation (LDA) and the deformed-jellium model.^{13,14} The most common assumption for describing the fission process of charged metal clusters is that small singly charged fragments (of three or nine atoms) evaporate from the cluster until a singly ionized cluster is left behind.^{9,15} Then it is possible to model the process as a chemical reaction by considering a static energy balance between reactants and products overcoming a reaction activation barrier.^{7,9,10,14,17}

One of the issues central in understanding the fission mechanism due to Coulomb forces is the determination of the appearance cluster size N_a , which is the smallest size at which a cluster supporting a charge of $2+$ or larger is observed experimentally. The minimum appearance size value is obtained at zero temperature when fission is spontaneous. This is the Bohr-Wheeler n_c parameter of the liquid-drop

model.¹⁷ Therefore, multiply charged clusters are intrinsically unstable if their size is below n_c . Above this size, clusters are metastable if their internal energy is lower than an energy barrier for fission that depends on the metal and the charge. If the cluster internal energy exceeds this energy barrier, then fission occurs. The range of metastable cluster sizes (appearance sizes) is quite ample. The largest appearance size is known as the critical size and this is the most frequently measured quantity.¹⁻⁴ Chandezon *et al.*¹⁰ observed a suite of critical sizes for Na clusters undergoing fission from different ion beam measurements and correlated these differences with temperature effects.

Local spin density calculations of doubly charged beryllium clusters with $N \leq 5$ (Ref. 18) have shown that small doubly charged clusters may exist in metastable states if their internal energy is lower than an energy barrier leading to a dissociation channel. The fragmentation process of very small Na_N^{2+} cluster ions containing up to 12 atoms [sizes below n_c (Refs. 19 and 20)] has been studied within the LDA for the electronic structure in conjunction with molecular dynamics (MD). However, this approach is computationally demanding and has not been used to investigate the fission mechanism of metastable multiply charged clusters with sizes above n_c . Molecular dynamics simulations aimed to describe realistic finite-temperature properties of larger systems, for example, clusters containing more or about 20 atoms, should meet two requirements: (i) a quantum mechanical foundation to describe the interaction between atoms and (ii) a high numerical efficiency. The first requirement is important because of the many-body character of the interatomic forces that enter in the description of the structural and thermodynamical properties. On the other hand, large-scale quantum mechanical simulations are highly computer intensive. Therefore, first-principles approaches are severely

limited to study vibrational, structural, and thermodynamic properties of large clusters. As an alternative, atomistic simulations are playing an increasingly important role in the design of modern materials. Most model potentials are empirical and their parameters are fitted to experimental values of bulk materials. Because the predicted structural material properties are as accurate as the interatomic potentials used, the development of improved model potentials is crucial. There have been several efforts that include averaged many-body effects fitted on first-principle calculations of both band structure calculations²¹ and small clusters potential energy surfaces.²² Model potentials describe well those properties associated with the structure and motion of the ionic atomic cores, which are much slower than the motion of the electrons.

We have applied a different many-body interatomic potential to describe sodium clusters, both the structure of neutral clusters and the fission mechanism of clusters multiply charged by 2+, 3+, and 4+.²³ These properties are structural and dynamical and therefore appropriate for study from an atomistic point of view. The class of many-body potentials is based on LDA calculations and the second moment approximation (SMA).^{24,25} The fission mechanism in hot charged metallic clusters, as in the nucleus, is based on the interactions between the ionic atomic cores. Our work²³ studies fission from a dynamical view, and for that we developed the best existing potential (to our knowledge) for sodium. These highly charged clusters undergo fission when they are hot at a certain size, the appearance size N_a . In our calculation we predicted the full range of appearance sizes of sodium clusters from its lower bound n_c (spontaneous fission at zero temperature) up to the critical size N_c attained at temperatures below the boiling point. Fission in the metastable cluster size region that spans between n_c and N_c was studied with nonequilibrium molecular dynamics by changing the internal energy of the multiply charged clusters. Multiply charged clusters larger than N_c are stable and do not fission. Our calculated critical sizes²³ are in excellent agreement with experiment.^{3,4,10}

In this work we present a systematics of interatomic potentials based on the LDA/SMA for K, Rb, and Cs and use these potentials to study the energetics, free energy, melting and boiling temperature, and surface energy of neutral clusters with 8 up to 309 atoms. We also study dynamically the fission mechanism of 2+, 3+, and 4+ cluster ions containing 10–160 atoms. This work tackles the fission process over a wide range of temperatures. Furthermore, we predict quantitatively the critical size for fission of alkali-metal clusters charged up to 4+. Our calculated critical sizes at high temperatures are in excellent agreement with experimental values for hot clusters.^{2–4,10} This is a confirmation of the importance of ionic atomic motions in the fission process. It is the first time, to our knowledge, that such an attempt has been carried out due to the difficulty of representing materials, such as the alkali metals, that are very soft. By including the dynamics of the atomic cores, our calculation represents a significant improvement over the liquid-drop model that describes the process only at zero temperature and assumes a structureless ionic cluster. In addition, we develop a size-temperature phase portrait that allows classification of the highly charged clusters in three phases: (i) clusters “stable to

fission” if the size is above N_c and the temperature is below T_c , (ii) clusters “metastable to fission” if the size is between n_c and N_c and the temperature is below a phase-separating line that spans between zero temperature and T_c , and (iii) “unstable clusters” if the size is between n_c and N_c and the temperature is above the phase line. We calculated the phase line for all the four metals under consideration. Fission only occurs in the metastable region, which is the region studied in this work. Multiple types of fragmentation processes occurring in the unstable region are not the subject of this work.

This paper is organized as follows. Section II describes the LDA band structure calculation leading to the establishment of the model potentials for Li, Na, K, Rb, and Cs. Section III describes the results for several bulk properties. The structure, energetics, and vibrational analysis of neutral Na, K, Rb, and Cs clusters are described in Sec. IV, including a visualization of the minimum energy structures of Cs clusters with 8 up to 20 atoms. Section V develops the molecular dynamics strategy used to study the fission mechanism at finite temperatures. Section VI describes the results obtained for all appearance sizes of clusters supporting charges of 2+, 3+, and 4+ (5+ in the case of Cs). The discussion in Sec. VII is followed by concluding remarks in Sec. VIII.

II. MANY-BODY POTENTIALS BASED ON LOCAL DENSITY BAND STRUCTURE

A. Local density calculation

First-principles calculations within the local density approximation of the total energy and electronic bands for both bcc and fcc crystals of the alkali metals Li, Na, K, Rb, and Cs were performed using an augmented-plane-wave (APW) method.²⁶ The band states were calculated self-consistently in the semirelativistic approximation with spin-orbit coupling neglected. The self-consistent semirelativistic calculations yielded the crystal potential, the charge density, and the eigenvalue sum, which were used in Janak’s expression for the total energy.²⁷ The exchange and correlation were treated by the Hedin-Lundqvist formalism.²⁸ The band calculations contained 55 k points in the irreducible Brillouin zone for the bcc structure and 89 k points for the fcc lattice.²⁶ The total energy was calculated for at least six different lattice parameters for each material and each crystal structure.

The APW total energy per atom of the crystal was expressed relative to the energy of an isolated atom calculated in the same approximation. Since it is well known that the total energy of isolated atoms is poorly described by the LDA, for the purpose of constructing the model potentials, we shifted the atomic energy so that the energy evaluated at the LDA equilibrium volume coincides with the experimental value of the bulk cohesive energy.²⁹ These energy shifts are 0.43, 0.21, 0.28, 0.19, and -0.10 eV for Li, Na, K, Rb, and Cs, respectively. In Table I we report the results of the calculated equilibrium lattice constants and bulk modulus along with the corresponding experimental values.^{29–31} The experimental cohesive energy E_b is also reported in the table. The calculated equilibrium lattice constants are within an error of about 5% and the bulk moduli are within an error of about 25% with experiment.

TABLE I. Lattice constant, bulk modulus, and melting temperature for alkali-metal clusters from our LDA and model potential calculations and from experiment. The last column is the experimental cohesive energy.

Element	bcc lattice constant (a.u.)			Bulk modulus (Mbar)			Melting temperature (K)		E_b (eV)
	LDA	Potential	Expt. ^a	LDA	Potential	Expt. ^b	Potential	Expt. ^c	Expt. ^a
Li	6.35	6.34	6.60	0.155	0.157	0.133	504.8	453.7	1.63
Na	7.68	7.63	8.11	0.094	0.087	0.074	332.9	370.9	1.13
K	9.53	9.52	9.9	0.047	0.048	0.037	270.8	336.8	0.93
Rb	10.17	10.16	10.60	0.037	0.037	0.029	270.8	336.8	0.85
Cs	10.93	10.91	11.42	0.020	0.020	0.023	300.4	301.6	0.80

^aReference 29.

^bReferences 30 and 31.

^cReference 36.

B. Model potentials

The criterion to construct the functional that describes the SMA (Refs. 24 and 25) many-body potentials is based on the functional that approximates the hopping integral in a tight-binding (TB) description. The TB approximation has been successfully proposed for most metals including the alkali metals.^{32–34} The TB eigenvalue equation is

$$(\varepsilon_{ia}^0 - E)|ia\rangle + \sum_{j \neq i} \sum_b t_{ab}^{ij}(r_{ij})|jb\rangle = 0, \quad (1)$$

where ε_{ia}^0 are the one-electron eigenvalues associated with one of the electrons of the atom at site i that occupies the orbital a . The hopping integrals $t_{ab}^{ij}(r_{ij}) = \langle ia|V_{ij}|jb\rangle$ include the site-site Coulomb interaction V_{ij} , which depends on the interatomic distance r_{ij} . For a system with N atoms, the total potential energy of the atomic ions is

$$U_{\text{coh}} = U_{\text{el}} + U_{\text{rep}}, \quad (2)$$

where U_{el} is the sum of the one-electron eigenvalues of the occupied states calculated from Eq. (1) and U_{rep} describes the repulsive ionic interaction represented by the Born-Mayer potential

$$U_{\text{rep}} = \sum_i \varepsilon_0 \sum_{j \neq i} \exp\left[-p\left(\frac{r_{ij}}{r_0} - 1\right)\right]. \quad (3)$$

Analytical interatomic potentials for Li, Na, K, Rb, and Cs were constructed by using the SMA,^{24,25} which takes into account the essential band character of the metallic bond. Namely, U_{el} consists of a band structure term proportional to the effective width of the valence band given by the square root of the second moment of the local density states. The SMA is similar to the embedded atom formalism and inspired by the TB expression to represent the hopping integrals: $t_{ij}^{ab} = A_{ab} \exp(-d_{ab}r_{ij})$. In the SMA the cohesive energy of the crystal is given by an analytical expression composed of a sum of one-atom effective binding energies

$$U_{\text{coh}} = U_{\text{rep}} - \sum_i \left\{ \sum_{j \neq i} \zeta_0^2 \exp\left[-2q\left(\frac{r_{ij}}{r_0} - 1\right)\right] \right\}^{1/2}, \quad (4)$$

where the first term is Eq. (3). The second term is the attractive interaction representing the band structure treated in the SMA. In this work sums are taken over neighbors within 12

coordination shells in a crystal and over all atoms in clusters. In addition, r_0 is a free parameter, as suggested in Ref. 25. Thus the potential has five parameters.

In this work we fitted the parameters of Eqs. (2)–(4) to a LDA database that consists of the total energy as a function of the lattice constant for both bcc and fcc lattices. This represents a very significant improvement over previous SMA TB fits to experimental quantities rather than to LDA band structure. Therefore, these potentials are based on rigorous first-principles LDA results. Resulting values for the parameters are reported in Table II. The rms error of the fit is very small, as shown in the last column of this table. No alternative empirical parametrization of this potential has been offered in the literature.

III. BULK PROPERTIES OF ALKALI METALS

We calculated several crystal properties using the present model potential functions. The bulk modulus, equilibrium lattice constant, and melting temperature are reported in Table I, where values can be compared to the LDA values for the first two properties. The melting temperature for the bcc and fcc crystals were calculated from Lindemann's criterion.³⁵ Lindemann's criterion states that at the melting temperature, the average amplitude of vibration $\langle u^2 \rangle$ should be about 15% of the nearest-neighbor distance d . In the harmonic approximation the vibration displacement of every atom u_i is a linear combination of the normal modes ξ_j such that

$$\langle u_i^2 \rangle = \sum_{j=1}^{3N-6} |e(i,j)|^2 \langle \xi_j^2 \rangle = \sum_{j=1}^{3N-6} |e(i,j)|^2 \frac{kT}{m\omega_j^2}, \quad (5)$$

TABLE II. Model potential parameters in Eqs. (3) and (4).

Element	ε_0 (mRy)	ζ_0 (mRy)	p	q	r_0 (a.u.)	rms (mRy)
Li	2.4450	23.889	7.75	0.737	5.490	0.016
Na	1.1727	21.398	10.13	1.30	6.99	0.014
K	1.51	19.30	10.58	1.34	8.253	0.009
Rb	1.43	18.12	10.48	1.40	8.81	0.004
Cs	1.51	17.80	9.62	1.45	9.44	0.021

where $e(i,j)$ is a matrix showing the contribution of the normal mode ξ_j with frequency ω_j to the particle displacement u_i and k is Boltzmann's constant. The melting temperature is then

$$T_m = \frac{Nm(0.15d)^2/k}{\sum_{i=1}^{3N} \sum_{j=1}^{3N-6} e(i,j)^2/\omega_j^2}, \quad (6)$$

where m is the atomic mass, $d=\sqrt{3}a/2$, and a is the lattice constant for the bcc crystal symmetry. Using our model potential, we are able to find the normal modes of clusters and crystals. For crystals, we chose a number of symmetrical \vec{k} -mesh points in the Brillouin zone and took the average with the corresponding weights. Calculated values of T_m are given in Table I and compared to experiment.³⁶

We also calculated the Grüneisen constant, which is defined as

$$\gamma_i = -d(\ln \omega_i)/d(\ln V) = (V/\omega_i)(d\omega_i/dV), \quad (7)$$

where $V=a^3/2$ is the volume per atom at equilibrium in the bcc crystal. This constant is useful in discussing anharmonic effects in solids. We calculated γ as the arithmetic average of γ_i for each normal mode. This is equivalent to a spherical average in k space, although for some effects it may be necessary to consider the dependence of γ on specific \vec{k} directions. The calculated Grüneisen constant is 1.61 and 1.54 for sodium and potassium, respectively. The experimental values are 1.4–1.7 (Ref. 37) and 1.34,³⁸ respectively.

IV. NEUTRAL ALKALI-METAL CLUSTERS

The model potential discussed in Sec. II B gives information on the structure of the material, where the atoms are located, and how they displace about their positions. Since the ionic atomic core motions are about two orders of magnitude slower than the electronic motions, the atomic ions move in the averaged field created by the electrons. This mean behavior is taken into account through the SMA, which gives the width of the valence band. However, the potential does not explicitly address the grouping of one-electron levels within the valence band that is observed in alkali-metal clusters. This grouping of states creates peaks in the density of states. As the clusters grow larger and tend to have bulklike sizes, these oscillations in the density of states disappear. A simplified representation of this effect is obtained by the spherical jellium model for clusters that totally neglects the structure of the atomic ions. Under the spherical jellium model, electron-subshell closings occur when the number of electrons N_e in the valence band is 2, 8, 18, 20, 34, 40, 58, 68, 90, 92, 106, 132, 138, 168, etc. Therefore, clusters containing those numbers of electrons in the valence band are expected to be more stable than others. In the jellium model of clusters, there is an accidental degeneracy where many of these electron subshells bundle together giving rise to shells.³⁹ These shells constitute peaks in the density of states. In the jellium calculations these peaks can be shifted by changing the density of the jellium. Shells occur when the number of valence electrons in the cluster is consistent with groupings of electron-subshell closings at ap-

TABLE III. Wigner-Seitz radius r_s of bcc crystals, calculated surface energy ϵ_s from Fig. 1 and Eq. (9), calculated surface tension σ at $T=0$, and experimental surface tension.

Element	r_s (a.u.)	ϵ_s (eV)	σ (eV/Å ²) at $T=0$ K	σ (eV/Å ²) (Expt. ^a)
Na	3.76	1.076	0.0217	0.0125
K	4.69	0.852	0.0110	0.0069
Rb	5.00	0.7574	0.0086	0.0056
Cs	5.37	0.6714	0.0068	0.0044

^aReference 36.

proximately $N_e=8, 20, 40, 58, 90, 132, 168$, etc.^{40,41} Since the density of the jellium depends on the mass of the alkali metal, the observed shell structure differs from one metal to another.^{42–45}

For completeness, in order to study the binding energy of metallic clusters, it is important to include an electronic term to describe subshell closings in a semiclassical description such as the one that emerges from the use of model potentials. According to Strutinsky's theorem,⁴⁶ the energy of the interacting fermion system can be divided into a smooth part and an oscillating part associated with the shell correction. The smooth part varies slowly with particle number and can be represented by the model potential introduced in Sec. II B. The shell correction contains all the oscillations coming from the bundling of energy levels. Therefore, we have added a shell term to the potential described in Sec. II B, to model the higher stability of clusters of size N that contain a number of valence electrons N_e corresponding to subshell closings:

$$E_N = \frac{U_{\text{coh}}}{N} - \frac{0.2}{N} \sum_K N_{e_K}^{1/3} \delta(N - N_{e_K}), \quad (8)$$

where U_{coh} , given in Eqs. (2)–(4), represents the structural contribution to the binding energy per atom, units are in eV, K is the subshell index, and N_{e_K} is the number of electrons that close the K subshell. The last term is a sum of delta functions peaked at each subshell index and weighted by a dependence on $N_{e_K}^{1/3}$ to reflect the contribution of the surface curvature to the cluster binding energy per atom. Therefore, this last term is a pure electronic contribution to the binding energy. Each δ function is represented by $\delta_e / [\delta_e^2 + (N - N_{e_K})^2]$, where $\delta_e = 1/n_K$ and n_K is the principal quantum number of the K subshell. The factor 0.2 is an estimate based on *ab initio* calculations for sodium.^{47,48}

Under this interatomic potential function, large clusters containing up to about 10 000 atoms, nonrelaxed and spherically carved from perfect bcc and fcc lattices, are less stable than icosahedral clusters. Martin⁴⁹ has confirmed experimentally that clusters larger than 1500 atoms have icosahedral structure. For smaller alkali-metal clusters, the structure obtained with the present model potential is expected to work best when the coordination shell of each atom is well populated.

In what follows we report results for clusters with less than 13 atoms along with those for clusters of up to 309 atoms. However, results for the small clusters are more ap-

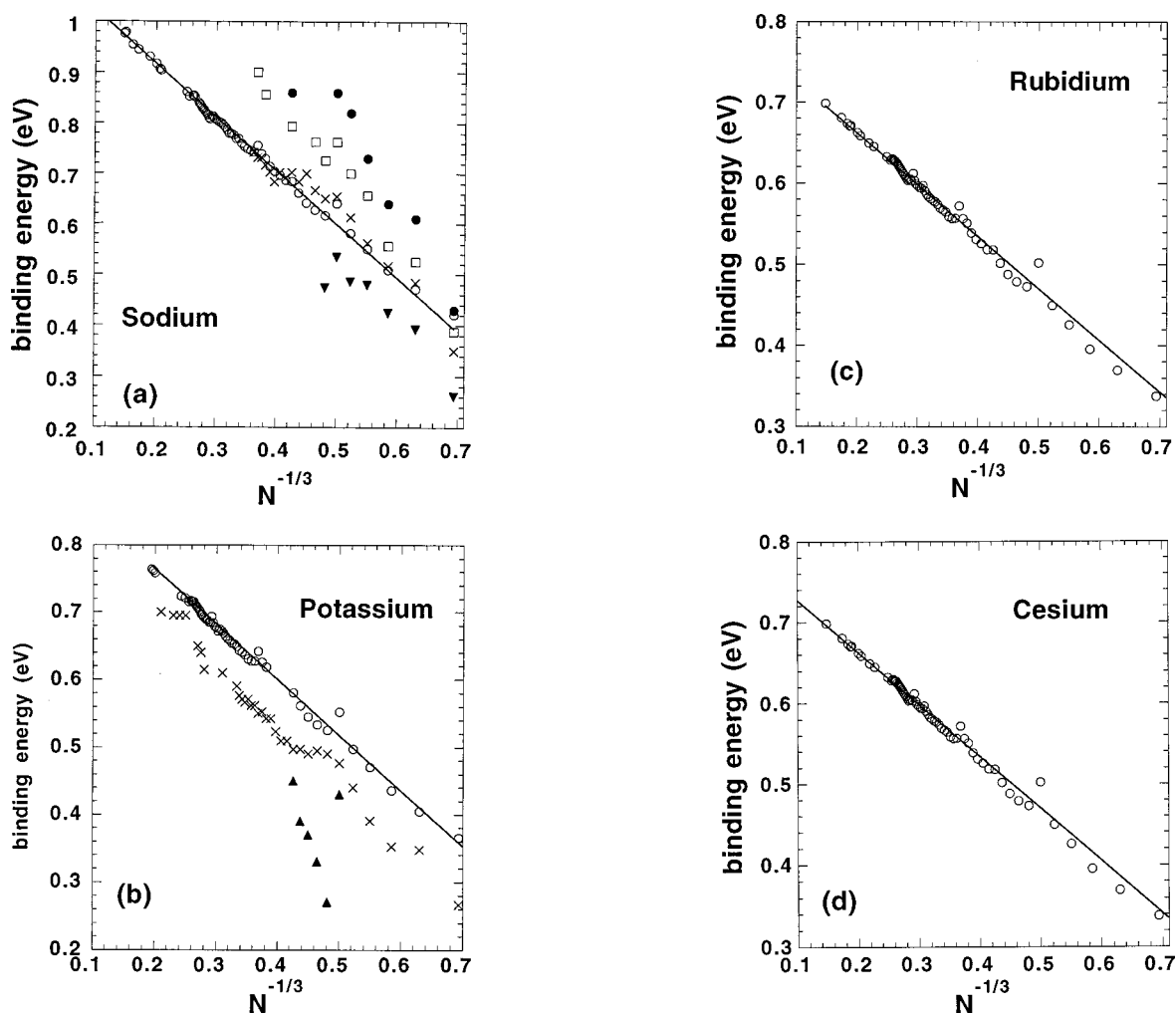


FIG. 1. Cluster binding energy per atom versus $N^{-1/3}$. (a) Sodium clusters: this work (circles) and experiment from Ref. 7 (crosses), Ref. 47 (triangles), Ref. 48 (squares), and Ref. 51 (solid dots). (b) Potassium clusters: this work (circles) and experiment from Ref. 7 (crosses) and Ref. 52 (triangles). (c) Rubidium clusters: this work (circles). (d) Cesium clusters: this work (circles). The solid line in all four figures is the fit to our calculation.

proximate. The minimum energy geometrical configuration of clusters in this size range was obtained by a dynamical simulated annealing process.⁵⁰ Clusters were annealed using MD and a time step of $0.02t_0$, where $t_0 = \sqrt{mr_0^2/E_b}$, m is the mass of the alkali metal, and r_0 and E_b are given in Tables I and II. Annealed clusters were finally minimized with a Newton-Raphson algorithm.

Figure 1(a) shows the binding energy $|E_N|$ for sodium calculated from Eq. (8) (circles) as compared with experiment⁷ (crosses) and with three first-principles calculations^{47,48,51} (triangles, squares, and closed circles). Our potential gives satisfactory binding energies for the smallest clusters and excellent agreement with experiment for larger clusters. Figure 1(b) illustrates an equivalent analysis for potassium, showing again good agreement of our calculation (circles) with experiments⁵ (crosses) and a comparison to previous calculations.⁵² Figures 1(c) and 1(d) show the results for rubidium and cesium. To our knowledge, there are no other calculations or experiments of binding energies for these two materials. Clusters where $N=N_{E_K}$ are noticeably more stable due to the shell effect. Figure 2 gives several minimum energy geometries obtained for small cesium

clusters, whereas Fig. 3 illustrates four almost degenerate structures obtained for clusters with 20 atoms. Several of the lowest energy Cs isomers shown in Fig. 2 are the same as those reported for sodium.⁴⁸ However, Fig. 2 illustrates several other structures not reported previously. The alkali-metal clusters are very soft and many different structures were found within a few kilocalories of energy. For example, the energies of the four structures for Cs_8 in Fig. 2 are bundled within 0.2 kcal/mole, there are eight different Cs_{18} structures within 1.4 kcal/mole of the minimum energy structure, while there are four different Cs_{20} structures within 0.14 kcal/mole and seven different Cs_{40} structures are found within 0.24 kcal/mole. The larger the clusters, the greater the number of isomers that are almost degenerate in energy. Structures of Na, K, Rb, and Cs clusters not reported here are reported elsewhere as part of a database with approximately 1000 entries constructed with all the minima discovered for these four metals.⁵³ Cesium structures different from those in Ref. 48 are, following the energy ordering in Fig. 2, the second Cs_8 , second Cs_9 , first Cs_{10} , and all of the Cs_{11} and Cs_{12} . The third Cs_{20} structure in Fig. 3 has been found previously for sodium.⁴⁸ The other three have not yet been re-

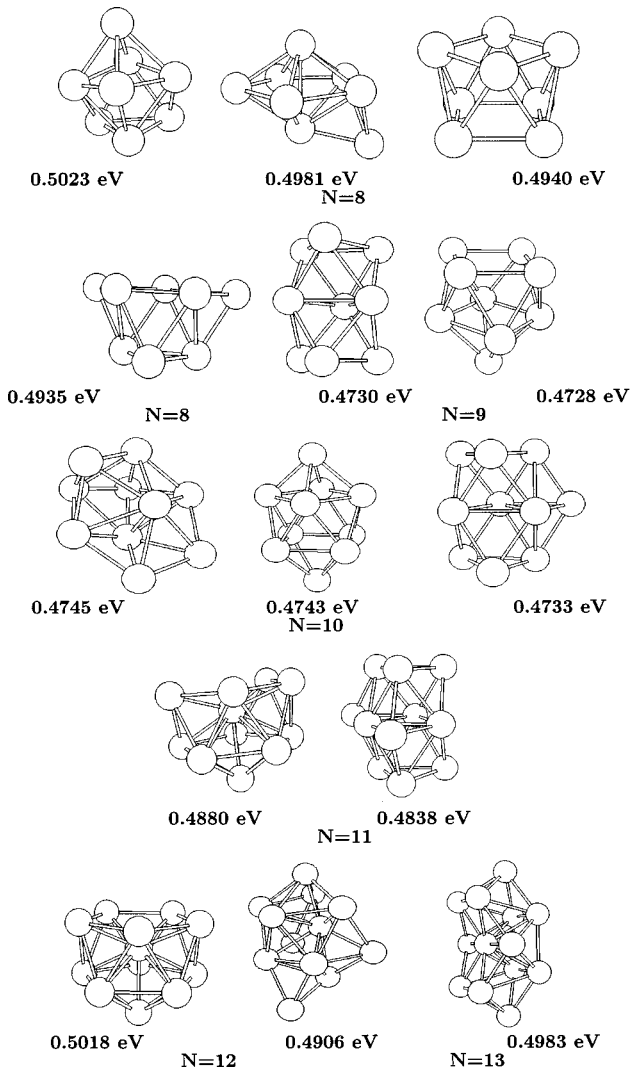


FIG. 2. Structure and binding energy/atom of the lower energy structures found for cesium clusters with $N=8-13$.

ported as far as we know. We find that there are three predominant motifs; the Cs_7 pentagonal bipyramid, the Cs_6 pentagonal pyramid, and the octahedron, that repeatedly appear with different relative orientations in the structure of the large clusters. It is noticeable that the growth does not take place around the icosahedral seed. This is in agreement with the study that emerges from the sodium LDA calculations.⁴⁸ However, we find that Cs_{13} , Cs_{55} , Cs_{147} , and Cs_{309} icosahedral structures are the most stable for that size, although the search for the larger clusters might not have been exhaustive. The icosahedral structures are relatively more stable than their isomers and, contrary to other cluster sizes, there is a small energy gap between the icosahedral structure and the next isomer found. For example, this gap is 0.46 kcal/mole for Cs_{13} and decreases to 0.1 kcal/mole for Cs_{55} . The Cs_{13} in Fig. 2 depicts the first isomer above the icosahedron.

As illustrated in Figs. 1(a)–1(d), our calculated binding energies/atom $|E_N|$ are organized on a straight line when plotted vs $N^{-1/3}$, in excellent agreement with experimental results (within 5–10%). In addition, the extrapolation of this line to the bulk leads to E_b , the cohesive energy of the bulk. This is not an obvious result. Because of this linear behavior, we can predict an estimate of the surface energy ϵ_s by fitting to the expression

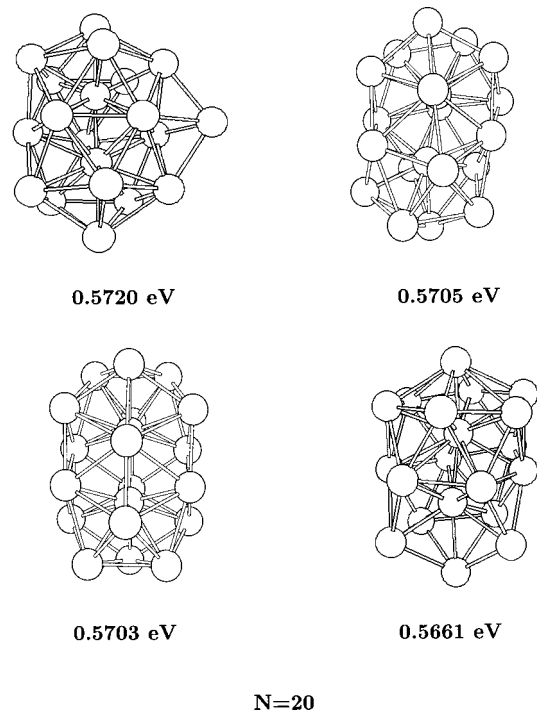


FIG. 3. Four quasidegenerate minimum energy structures found for Cs_{20} with their binding energies.

$$|E_N| = E_b - \epsilon_s N^{-1/3}, \quad (9)$$

where the N -independent term E_b is reported in Table I. The second term is the surface term proportional to $N^{2/3}$ typical of metals. The solid line in Figs. 1(a)–1(d) shows this fit. The fit yields a surface energy of $\epsilon_s = 1.076, 0.852, 0.7574,$ and 0.6714 eV for Na, K, Rb, and Cs, respectively. Relation (9) is very interesting and shows that for alkali-metal clusters *all* the structural binding energy comes from the surface term. The smaller the cluster, the larger the surface contribution. This behavior is certainly not obtained for other materials such as silicon.⁵⁴ We conclude that metal clusters in the size range of this study behave as surfaces. The surface tension of these metallic objects at zero temperature was calculated by using $\epsilon_s = 4\pi r_s^2 \sigma$, where r_s is the Wigner-Seitz ra-

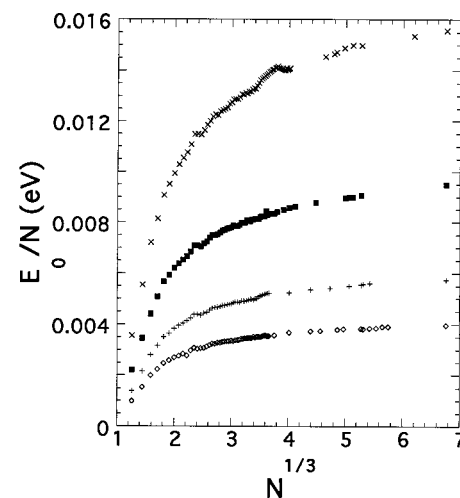


FIG. 4. Zero point energy per atom vs N for Na (crosses), K (closed squares), Rb (pluses), and Cs (diamonds) clusters.

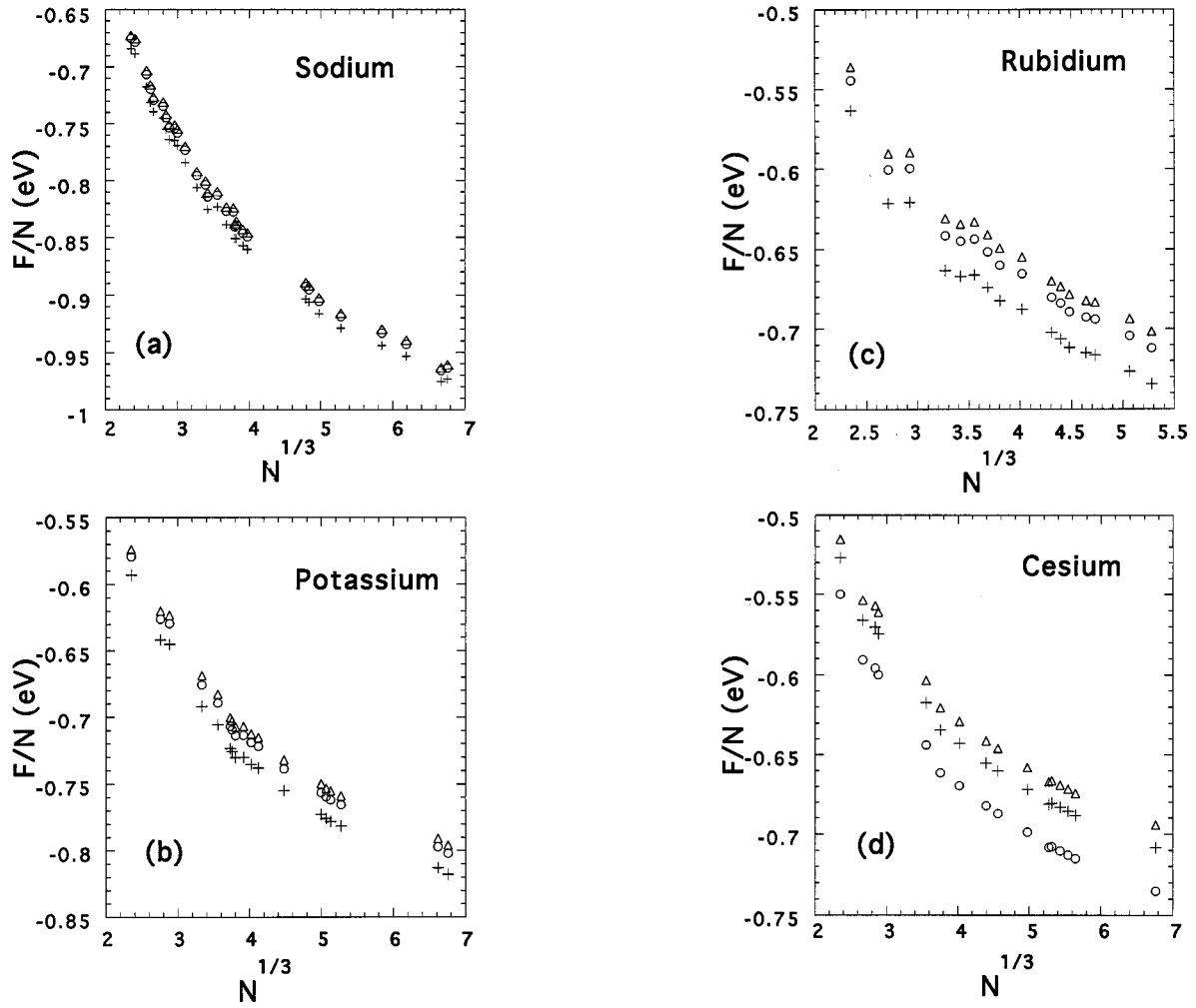


FIG. 5. Free energy per atom vs cluster size $N^{1/3}$ for (a) Na, (b) K, (c) Rb, and (d) Cs at three different temperatures: 5 K (triangles), 55 K (circles), and 105 K (pluses).

dus. Results are given in Table III. Considering that surface tension decreases with increasing temperature, our results are consistent with experimental values for the bulk (last column of Table III).³⁶

Normal mode calculations for clusters of all sizes were also obtained, such that the $3N-6$ normal mode frequencies for every cluster size N are available.⁵³ Figure 4 illustrates the trend of the zero point energy as a function of cluster size. Given that these clusters are very soft and that absolute energy differences between binding energies of two different isomers are so close, Fig. 4 shows that the zero point energy is not negligible and presents a strong dependence with cluster size up to about $N=60$. This zero point energy has systematically been neglected in studies of energy balance at zero temperature where clusters are assumed to be structureless. Additionally, we studied the cluster Helmholtz free energy in the harmonic approximation

$$F = - \sum_{i=1}^{3N-6} kT \left[\ln \left(\frac{\exp(-\hbar \omega_i / 2kT)}{1 - \exp(-\hbar \omega_i / kT)} \right) \right] + E_N N, \quad (10)$$

where ω_i are the normal mode frequencies for a cluster of size N . Results of the free energy per particle at three low temperatures for sizes $13 \leq N \leq 309$ are shown in Figs. 5(a)–

5(d) for Na, K, Rb, and Cs, respectively. It is apparent that as clusters grow larger they become more stable and their free energy tends slowly toward the bulk value. The relative importance of the shell contribution vanishes as the cluster grows larger.

Furthermore, the melting temperature T_m of clusters was calculated as a function of cluster size within Lindemann's approximation Eq. (6), assuming that the ratio between the mean atomic displacement in the clusters and r_0 is 0.15. Knowing both F and T_m permits tracing of a phase portrait in the plane F/N vs $N^{1/3}$. This portrait is given in Fig. 6, where each point indicates the free energy per particle at T_m for every given size. Solid lines are drawn to guide the eye. Below the line clusters are liquidlike and above the line clusters are solidlike. This phase portrait shows clearly that the solidlike phase increases its stability as the cluster grows larger.

The same trend described by Eq. (9) can be used to estimate the boiling temperature of an N -atom cluster by assuming that

$$T_b = T_0 \left(1 - \frac{\epsilon_s}{E_b} N^{-1/3} \right), \quad (11)$$

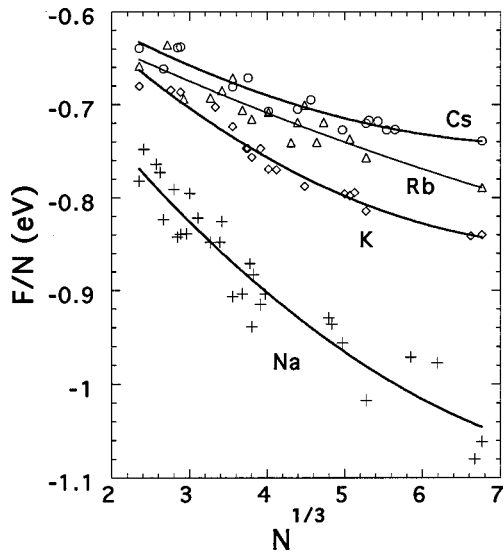


FIG. 6. Portrait in the plane of free energy vs cluster size $N^{1/3}$. Each point is the free energy at the melting temperature for each cluster size: Na (pluses), K (diamonds), Rb (triangles), and Cs (circles). Lines guide the eye.

where T_0 is the boiling temperature of the bulk. Tables I and III give the bulk binding energy E_b and the cluster surface energy ϵ_s , respectively.

V. FISSION OF MULTIPLY CHARGED ALKALI-METAL CLUSTERS

In this section we describe the use of our cluster potential to simulate the fission mechanism of multiply ionized clusters in the size range $10 \leq N \leq 160$. A dynamical study with MD of the fission mechanism is very important because the entropic effects are automatically included. Fission is a process where information on the structure of the clusters is important because the largest contribution to the cluster entropy comes from the atomic motions. Multiply ionized alkali-metal clusters are usually produced using the technique of multistep photoionization. These highly ionized clusters that have lost two or more electrons are very hot, with temperatures close to the boiling point of the metal. At these high temperatures the motion of the atoms in the charged cluster are liquidlike and the atoms visit many positions within the available volume of the cluster. There are numerous experiments available on the critical size to undergo fission. Therefore, one of the aims of our simulation is to obtain dynamically the critical size and temperature.

In this simulation, we assume that the positive charge is distributed equally among the atoms in the cluster by assigning a point fractional effective charge $q = Qe/N$ to each atom. Thus the deficiency of electrons is delocalized over the cluster irrespectively of where the atoms are located. Within this picture, a positively charged cluster is represented by N bonded atoms, each of which holds a charge $q+$ that interacts with all other charges, polarizes the material creating induced dipoles on each atom, and further interacts with those induced dipoles. Because the charge distribution is uniform, charge homogeneity is preserved and the cluster is electrically isotropic, much as are fluids and amorphous sol-

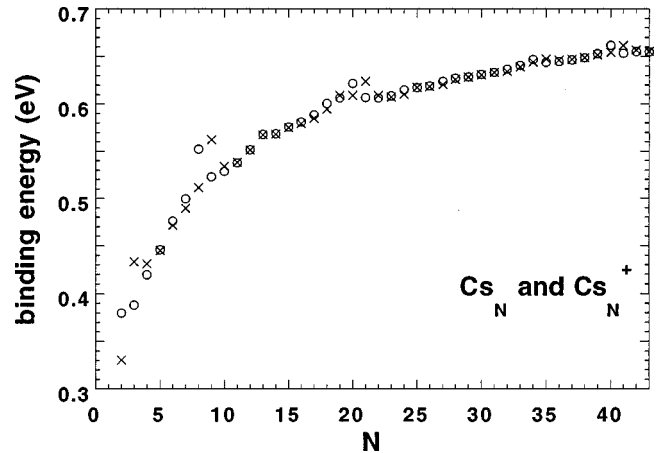


FIG. 7. Binding energy per atom of neutral (circles) and singly charged (crosses) cesium clusters.

ids. In addition, this model is consistent with the findings for sodium⁴⁸ concerning the spherical average of the electron density. This average shows that the negative charge in the cluster is almost uniform, which suggests that the positive charge should also be uniform to account for charge neutrality.

The Hamiltonian to represent a charged cluster with total charge $Qe = \sum_i q_i$ is

$$H = \frac{1}{2} \sum_i m v_i^2 + E_N + \frac{C}{2} \sum_{\substack{i,j \\ i \neq j}} \left[\frac{q_i q_j}{r_{ij}} - \frac{q_i^2 \alpha}{r_{ij}^4} \right], \quad (12)$$

where the v_i and m are the ion velocities and masses, E_N is given in Eq. (8), q_i are the effective charges of the ions, and α is the polarizability of ions: 0.312, 0.9, 1.7, and 2.5 \AA^3 for Na, K, Rb, and Cs, respectively.²⁹ The constant C is zero for neutral clusters and one when the cluster is charged.

First the above Hamiltonian was used to simulate singly charged clusters ($Q=1$) at zero temperature. These singly ionized clusters are stable. To that purpose we followed a procedure similar to the one described for neutral clusters to find the structures with minimum energy. Figure 7 shows the results on the binding energy of the singly ionized cesium clusters (crosses) compared to the binding energy of neutral clusters (circles). The shell closings are clear and the clusters with $N=9, 21, 41, \dots$ are more stable than their neighboring sizes. Similar observations were obtained for all the other metals. It is worth noting that the effect of a single charge changes the structure of the very small clusters. However, clusters with more than $N=10$ keep the same geometry when singly charged. The overall binding energy of the charged clusters is a few kcal/mol higher than for the neutral clusters, in agreement with previous calculations for sodium.⁴⁷

Simulations were performed using MD and Eq. (12). To describe the fission process we define two additional parameters: (i) a maximum atomic distance from the cluster center of mass R_{\max} and (ii) a maximum bond length R_b defined as r_0 incremented by the maximum averaged amplitude of atomic vibrations at a given temperature. R_b is set to about $2.6r_0$ and R_{\max} to approximately $10r_0$ for clusters with $N \leq 150$. A ‘‘cluster’’ is defined as that aggregate of N atoms

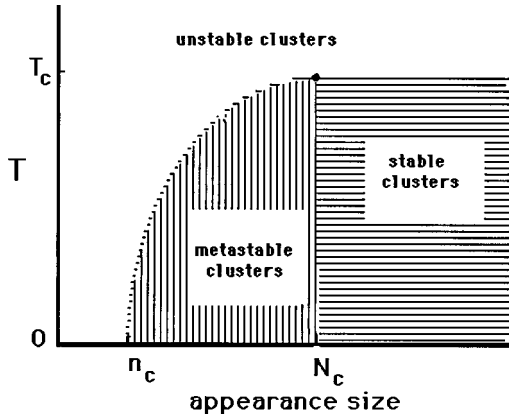


FIG. 8. Phase diagram for the fission process. Three regions are identified corresponding to unstable, metastable, and stable clusters. The critical point is characterized by (T_c, N_c) .

held together by the potential energy E_N with interatomic distances smaller than R_b . Neutral clusters ($C=0$) at low enough temperatures are exclusively composed of bonded atoms. Notice that the nearest-neighbor interatomic distances at zero temperature are necessarily smaller than R_b . By monitoring a larger characteristic interatomic length, we are able to observe the fission when it has already taken place and the two fragments are already separated, i.e., the shortest distance between the fragments is larger than R_b . For charged clusters ($C=1$) fission occurs when the cluster size is too small to sustain the charge.

The experimental conditions, as described by Martin and co-workers,^{2-4,49} are such that when measurement occurs some clusters undergo fission, but also there are other clusters that evaporate single neutral atoms. Temperatures in the experiment are very close to the boiling point. In this work we have not attempted to describe the evaporation process of the multiply charged clusters mostly because of the lack of information on how the distribution of charge is affected when a neutral atom is stripped from the cluster. For that reason in the computer experiment we only reach a maximum working temperature (close to boiling). This maximum working temperature is associated to the highest temperature that we could attain by heating a cluster before a single atom separates from the cluster. If the distance from any single atom to all other atoms is larger than R_b and its distance from the cluster center of mass is larger than R_{\max} , the simulation is stopped, the event is discarded, and another simulation is started from another configuration of a cluster of equal size (or of size $N-1$). Typical values of R_{\max} are between $9r_0$ and $12.5r_0$, depending upon the size. With the elimination of these events, we can ensure that our analysis is not based on evaporative conditions.

The strategy for the fission computer experiments is the following. First, the neutral cluster [$C=0$ in Eq. (12)] is equilibrated at a low temperature. Second, the neutral cluster is slowly heated to about 150 K and equilibrated at that temperature. Third, the cluster is charged instantaneously by switching $C=1$ and the simulation is continued to 25 000 time steps. Fourth, the charged cluster is heated by increasing its temperature in a steplike fashion from 150 K until the cluster undergoes fission. At each intermediate heating step, the dynamics is continued for 10 000 time steps and mean

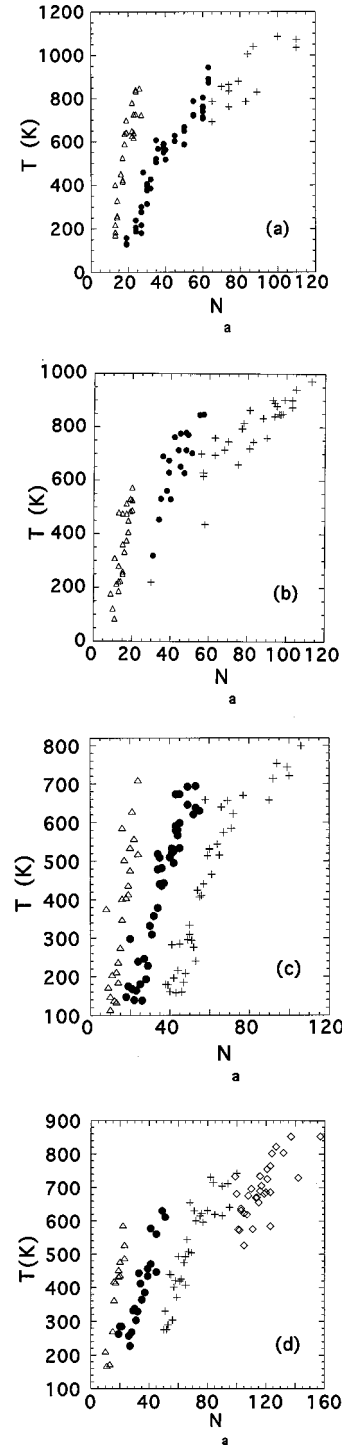


FIG. 9. Cluster temperature vs appearance size N_a for multiply charged clusters of (a) Na, (b) K, (c) Rb, and (d) Cs: $Q=2$ (triangles), $Q=3$ (closed circles), $Q=4$ (pluses), and $Q=5$ (diamonds).

quantities are averaged over that time interval only. This four-stage process is repeated for every cluster size N and for every total charge Q . The computer experiment is terminated at a maximum size $N=N_c$ if for the $N+1$ case we discarded five events in which one atom was beginning to strip from the cluster. Relevant quantities such as the temperature at which fission occurs are kept on file.

Following this procedure, the critical size N_c corresponds to that size at which the cluster undergoes fission and is at

TABLE IV. Calculated spontaneous fission size n_c , critical size N_c , and critical temperature T_c , for $Q=2+$, $3+$, and $4+$. The last column lists the experimental results from Ref. 4.

Element	Q	n_c			N_c			T_c (K)			N_c (Expt. ^a)		
		2	3	4	2	3	4	2	3	4	2	3	4
Na		11	20	36	27	63	110	848.3	945.4	1085.6	27	63	123
K		12	21	33	20	57	113	572.6	847.9	971.6	20	55	110
Rb		11	21	35	24	53	106	628.6	694.3	799.2	19	50	110
Cs		12	19	36	23	51	100	586.8	630.8	742.8	19	49	94

^aReference 4.

the highest attainable temperature T_c . The appearance size N_a is that size at which the cluster fissions at temperatures below T_c . Sizes $N_a \leq N_c$ correspond to metastable clusters. The spontaneous fission at zero temperature was studied as well. For that purpose, the cluster was charged at zero temperature and the MD simulation was continued for 5×10^6 time steps until the cluster fissioned. The maximum size at which clusters at zero temperature undergo fission is n_c , very similar to the Wheeler-Bohr parameter,¹⁷ except that here it is obtained dynamically. The highest appearance size, or critical size N_c , is attained at temperatures T_c that are comparable to the boiling point of the corresponding material.

The previous analysis allows us to depict a phase diagram for the fission mechanism as shown in Fig. 8 for a fixed charge. Three phases are apparent in this diagram corresponding to stable, metastable, and unstable clusters depending upon their size and temperature. The metastable phase corresponds to clusters that are not hot enough to undergo fission. This region is bounded by two typical points (N_c, T_c) and ($n_c, 0$) in the phase plane. The first point corresponds to critical quantities. The second point characterizes the spontaneous fission. Both points depend on Q and on the metal. We were able to determine the phase boundary line that separates the metastable from the unstable phases. This is important because now researchers can distinguish between phenomena associated with the different phases. In other words, fission only occurs when passing from the metastable to the unstable phase. Within the unstable region there is a myriad of possible fragmentation mechanisms and/or evaporation channels that make the clusters unstable. In the stable phase below the critical temperature the clusters do not undergo fission. Earlier dynamical calculations have only been performed in the unstable phase below n_c .¹⁹

VI. TEMPERATURE DEPENDENCE OF THE FISSION PROCESS

The MD results depicting the phase diagram for the fission of Na, K, Rb, and Cs clusters for each value of Q are provided in Figs. 9(a)–9(d). It is seen that as the temperature increases the appearance size increases up to N_c , which corresponds to T_c . At the critical size the temperature T_c is near the boiling temperature, as confirmed experimentally.^{4,49} Notice that it is only at these high temperatures that the fission and evaporation processes could coexist. There was no evidence in our simulations that at temperatures below T_c sub-

limination occurs, as was suggested by Martin.⁴⁹

In the low-temperature region of the phase diagram, Fig. 8 is the spontaneous size n_c , which is also an important quantity. Clusters smaller than n_c are unstable even at zero temperature. In the liquid-drop model (LDM),^{9,17} the Bohr-Wheeler parameter n_c is given by

$$n_c^{\text{BW}}(Q) = \frac{8.16Q^2}{\epsilon_s r_s} + 1. \quad (13)$$

In the LDM the values of the surface energy constant ϵ_s and the Wigner-Seitz radius r_s are taken from the bulk. However, in Sec. IV we obtained an estimate of ϵ_s for clusters as shown in Table III in the correct units. Therefore, we can calculate n_c^{BW} more realistically and compare it with the dynamically obtained n_c .

A. Sodium

Figure 9(a) illustrates our results for $Q=2+$ (triangles), $3+$ (closed circles), and $4+$ (crosses). Each point shows the highest temperature reachable by a cluster of a given size and charge that undergoes fission without evaporation. In the figure, points for each charge build up the phase boundary line that separates the metastable from the unstable phases. As we mentioned before, this phase boundary line depends on the charge and on the metal. Therefore, Fig. 9(a) summarizes three phase diagrams. Values of n_c , N_c , and T_c are given in Table IV. For each cluster size, several calculations were performed by choosing different initial times to charge the equilibrated cluster. Typical lifetimes before fission are on the order of several nanoseconds. As is evident from Fig. 9(a), the critical size is 27 for $Q=2$, 63 for $Q=3$, and 110 for $Q=4$. The first two results are in perfect agreement with the experimental observations of 27 ± 1 and 63 ± 1 .^{3,4} In the case of $Q=4$ our critical size is 110, whereas there are several experimental values reported: 123 ± 2 ,⁴ 122 ± 2 ,¹¹⁸ 118 ± 2 , and 115 ± 5 .¹⁰

The boiling temperature of bulk sodium is 1156.1 K. The estimated cluster boiling temperatures from Eq. (11) are 789, 879, and 926 K for $N_c=27$, 63, and 110 sodium clusters corresponding to $Q=2$, 3, and 4. The percent difference between T_c (see Table IV) and the estimated boiling temperatures is less than 17%.

The dynamical spontaneous fission sizes n_c are reported in Table IV. The LDM n_c^{BW} parameters estimated with our results of ϵ_s are $n_c^{\text{BW}}(2)=9.1$, $n_c^{\text{BW}}(3)=19.2$, and $n_c^{\text{BW}}(4)$

=33.3 for $Q=2, 3$, and 4 , respectively. Differences between our MD and the LDM values for the spontaneous size using our values of the surface tension are around ± 2 .

B. Potassium

Results for potassium are shown in Fig. 9(b) for charges of $2+$, $3+$, and $4+$ depicted with triangles, closed circles, and crosses, respectively. Once again, points in the plot illustrate the boundary between the metastable phase and the unstable phase for each value of the charge. Table IV summarizes the results for n_c , N_c , and T_c . The critical sizes are 20, 57, and 113, in agreement with experimental values of 20, 55, and 110.^{3,4} The boiling temperature of bulk potassium is 1047 K. From Eq. (11) we obtain that estimates of the cluster boiling temperatures are 693.6, 797.8, and 848.6 K, corresponding to $N=20, 57$, and 113 . The maximum fission temperatures T_c are at most 17.4% off from the boiling temperature estimates. The MD calculated spontaneous fission sizes are 12, 21, and 33 for $Q=2, 3$, and 4 , respectively. Using Eq. (13) and our values of ϵ_s from Table III, the LDM values are $n_c^{\text{BW}}(2)=9.2$, $n_c^{\text{BW}}(3)=19.4$, and $n_c^{\text{BW}}(4)=33.7$. Again the difference between our MD results and the LDM values is less than ± 2 .

C. Rubidium

Figure 9(c) illustrates our results for rubidium clusters supporting a charge of $2+$, $3+$, and $4+$ with triangles, closed circles, and crosses, respectively. The boundary between the metastable and unstable regions is quite sharply determined as for the lighter metals. The corresponding critical sizes are 24, 53, and 106 (see Table IV), comparable to the experimental values of 19, 50, and 110.^{3,4} For this material, the boiling temperature of bulk rubidium is 961 K. From Eq. (11) we find that estimates of the boiling temperature are 664.1, 733.1, and 781.4 K for clusters containing $N=24, 53$, and 106 , respectively. These values can be compared with the highest reachable temperatures T_c reported in Table IV. Estimates of the boiling temperature and T_c agree within at most 5.4%. The MD calculated spontaneous fission sizes are reported in Table IV. Using Eq. (13) and our values of ϵ_s from Table III, the LDM parameters obtained are $n_c^{\text{BW}}(2)=9.6$, $n_c^{\text{BW}}(3)=20.4$, and $n_c^{\text{BW}}(4)=35.5$. These values are in agreement with our MD simulations values within ± 1 .

D. Cesium

Results for Cs are shown in Fig. 9(d) for $Q=2+$ (triangles), $3+$ (closed circles), $4+$ (crosses), and $5+$ (squares). The critical sizes N_c reported in Table IV are 23, 51, 100, and 157, respectively. The metastable and unstable phases are well separated by the points in the graph. The experimental results^{3,4} are 19, 49, 94, and 155, showing excellent agreement with the calculation. The boiling temperature of the bulk is 951.6 K. From Eq. (11) we find that the estimates of the cluster boiling temperature are 670.8, 736.3, and 779.6 K for $N=19, 49$, and 94 , respectively. Once again, T_c from Table IV compares well to these estimates. From Eq. (13) and values of ϵ_s from Table III, we obtain

$n_c^{\text{BW}}(2)=10.1$, $n_c^{\text{BW}}(3)=21.3$, $n_c^{\text{BW}}(4)=37.2$, and $n_c^{\text{BW}}(5)=57.6$. The differences from the MD values of n_c are less than ± 2 .

VII. DISCUSSION

The assumption of distributing the charge over all atoms in the cluster instead of distributing over the most external atomic layer is reasonable in the size range $N < 160$. Indeed, at low temperatures, clusters in this size range have about 75% of the atoms on the surface. Besides, clusters are not billiard balls, but rather their atoms are enclosed by a flexible surface that changes dramatically with temperature and time. Even a very symmetric cluster in this size range, the $N=147$ icosahedron, presents a faceted surface and only three atomic layers from the central atom. We know from tight-binding calculations of planar infinite metallic surfaces,⁵⁵ that when the material is negatively charged, the charge decays from the outermost atomic layer within a skin of 3–4 layers. In a cluster, the surface that encloses all atoms has a strongly inhomogeneous curvature that impacts in the charge distribution profile. Models, or calculations, of the profile of the positive charge distribution in clusters are unavailable in the size range $10 \leq N \leq 160$. Furthermore, the fission process involves temperatures near the boiling point, where all atoms have high mobility and migrate from side to side of the cluster. Under these circumstances the concept of “volume” atoms versus “surface” atoms becomes unclear. Because of the above reasons, we believe that simulation of the fission mechanism with a uniform positive charge distribution deserves investigation and marks an important step forward in the understanding of a complex nonequilibrium process.

We conclude from Fig. 9 that in the nanosecond time range, small clusters with size larger than n_c are able to sustain a charge $Q \geq 2+$ only at temperatures below $T_c(Q)$. A phase diagram allows for the distinction between stable, metastable, and unstable clusters. We predict the phase boundary line that marks the size-temperature threshold for a metastable charged cluster to undergo fission. Therefore, metastable charged clusters of a specific size can be heated up to a temperature consistent with this boundary line before undergoing fission.

When the fission takes place, in all the cases considered, two fragments were obtained. The ratio of the two sizes tends to be about one for even charges, $\frac{1}{2}$ for a charge of $3+$, and $\frac{2}{3}$ when the charge is $5+$. For higher charges the ratio tends to one. Our simulations support the concept of symmetric fission put forth by early models,¹¹ where the ratios of fragment masses and fragment charges are equal. In the simulations the size ratios, and therefore the charge ratios, were not perfectly symmetric, with departures as large as ± 8 atoms. This is without doubt due to the model of uniform charge distribution that we have adopted. For example, if N is an odd number and Q is even, exactly $N/2$ in each of the fragments cannot be attained with this model. Figure 10 illustrates with four snapshots one typical fission event for the case $\text{Cs}_{100}^{4+} \rightarrow \text{Cs}_{46}^{2+} + \text{Cs}_{54}^{2+}$ as a function of time and temperature. The two shades of gray in the graph have the following origin. Once the cluster underwent fission, breaking into two parts [Fig. 10(d)], the atoms in each fission fragment were given different colors. Once identified, the atoms

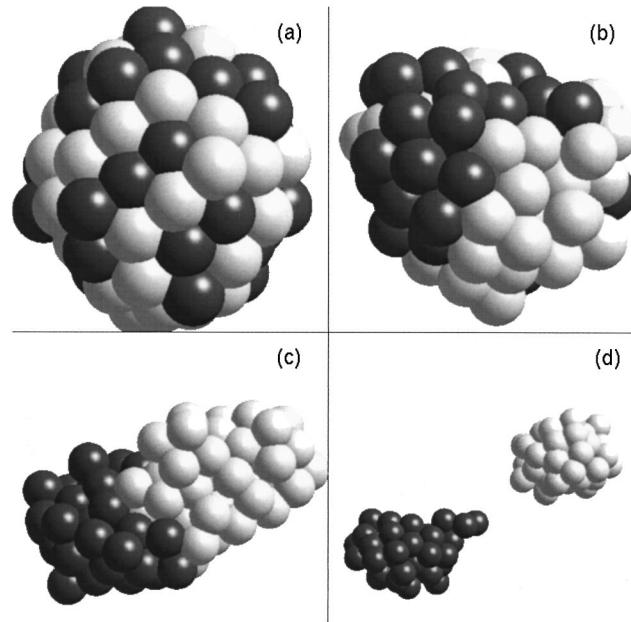


FIG. 10. Snapshots along a computer simulation of the fission process of Cs_{100}^{4+} . (a) $T=190$ K, time equals 30 ps; (b) $T=600$ K, time equals 330 ps; (c) $T=745$ K, time equals 400 ps; and (d) $T=750$ K, time equals 430 ps.

were given the same color in the other three graphs [Figs. 10(a)–10(c)]. As is apparent, the atoms that accommodate in each fission fragment were distributed randomly in the initial stages of the simulation at low temperature. A challenge for the future is to describe the charge distribution and its time dependence in a more detailed fashion. Work is in progress along those lines.

It is possible to combine our results for the alkali metals in a more unified fashion and compare them with a version of the LDM in which the parameters n_c and ϵ_s are taken from our results. The energy barrier/atom that a cluster needs to overcome for fission is given in the LDM (Refs. 9 and 17) by

$$V_f^{\text{LDM}} = 98\epsilon_s N^{2/3} (1 - n_c/N)^3 / 135, \quad (14)$$

where n_c is given in Eq. (13). In the LDM, the critical sizes are obtained by equating

$$V_f^{\text{LDM}} = |E_N|. \quad (15)$$

Here E_N is given in Eq. (9). This procedure yields $N_c^{\text{LDM}} = 20, 37, \text{ and } 61$ for Na; $24, 39, \text{ and } 58$ for K; $22, 39, \text{ and } 61$ for Rb; and $25, 36, \text{ and } 64$ for Cs, corresponding to $Q = 2+, 3+, \text{ and } 4+$, respectively. These values are far off from both the MD results for N_c (Table IV) and experiment. In fact the LDM is more successful in the prediction of n_c than in the prediction of N_c .

In the process of heating we are providing external thermal energy to the cluster that results in an increase of its temperature. Thus the increase of cluster temperature during the heating process is proportional to the energy barrier/atom V_f that the cluster has to overcome in order to undergo fission:

$$V_f(N_a, Q) = c_f [kT(N_a, Q) - kT_{\text{ref}}], \quad (16)$$

where c_f is a constant, $T(N_a, Q)$ can be extracted from Figs. 9(a)–9(d), and T_{ref} is approximately 150 K (initial tempera-

ture before the heating process started). The results of Figs. 9(a)–9(d) can be replotted under the perspective of Eq. (16). These shifted plots are given in Fig. 11, where $c_f = 1$. The solid line in this figure corresponds to the LDM fission barrier V_f^{LDM}/N [Eq. (14)], where ϵ_s and n_c were taken from Tables III and IV, respectively. As is apparent from Fig. 11, the LDM results are only in fair agreement for $Q = 2$, but fail for higher charges and heavier atoms.

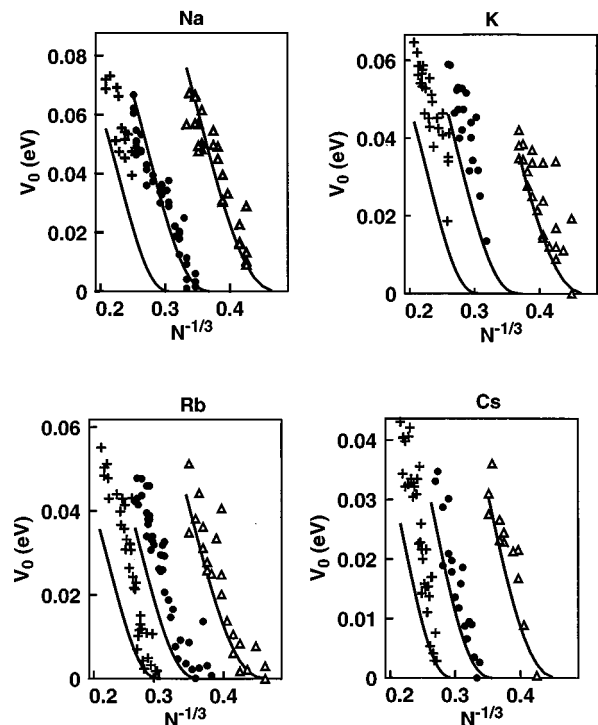


FIG. 11. Cluster temperature vs $N^{-1/3}$ for multiply charged Na, K, Rb, and Cs clusters. $Q = 2$ (triangles), $Q = 3$ (closed circles), and $Q = 4$ (pluses). The solid lines are the LDM from Eq. (14).

In addition, from the results of N_c tabulated in Table IV, one can seek the relation between $N_c(Q)$ and Q . Let us propose

$$\ln N_c = a_c \ln Q + b_c, \quad (17)$$

where a_c and b_c are constants. We obtain $a_c = 2.2$. This value is in excellent agreement with experiment,⁴ where a value of 2.3 was obtained. The Rayleigh classical macroscopic value is 2 (Ref. 56) and the averaged LDM value is 2.07.

All previous results indicate how important the thermal effects in the fission mechanism are. The thermal effects are a result of the atomic motions. The shell term has no effect on the fission mechanism. Furthermore, the dynamical description incorporates entropic effects that are absent in quantum mechanical calculations. Thus we emphasize that the fission process cannot be described solely at zero temperature.

VIII. SUMMARY

In this paper, we have constructed a series of potentials for the alkali metals from first-principles calculations. The potentials are shown to be very good in describing the structural properties of bulk metals and clusters in the size range $8 < N < 310$. The lattice constant, melting temperature, the vibration modes, the bulk modulus, and Grüneisen constant are in agreement with available experimental values. We

have also obtained the binding energy, zero point energy, and free energy at various temperatures and cluster sizes. The surface energy is calculated from cluster properties, which leads to a different method to obtain the surface tension at zero temperature.

The mechanism of fission due to highly charged metal clusters in the range $10 < N < 160$ was studied dynamically. Clusters undergo fission by breaking into two parts, in support of the symmetric fission concept. We show that the appearance size of highly charged clusters is temperature dependent and bounded between n_c , the spontaneous size at $T=0$, and N_c , the critical size at T_c . The comparison of N_c with experimental values is excellent. In addition, our values of n_c are in good agreement with the LDM when our value of the surface energy is used. We predict the size dependence of the energy barrier to undergo fission and explicitly show the failure of the LDM to describe it. Critical sizes scale with a power law of the total charge, with the exponent being in excellent agreement with experiment.

ACKNOWLEDGMENTS

The authors are grateful to Dr. T. Patrick Martin for very useful discussions and for his comments and careful reading of this manuscript. E.B.-B. acknowledges support from the Office of the Provost at GMU for sponsoring the funding allocated to Y.L.

*Electronic address: eblaiste@gmu.edu

¹O. Echt and T. D. Märk, in *Clusters of Atoms and Molecules*, edited by H. Haberland (Springer, Berlin, 1994), Vol. II, p. 183.

²U. Näher, H. Göhlich, and T. P. Martin, *Phys. Rev. Lett.* **68**, 3416 (1990).

³T. P. Martin, U. Näher, H. Göhlich, and T. Lange, *Chem. Phys. Lett.* **196**, 113 (1992).

⁴U. Näher, S. Frank, N. Malinowski, U. Zimmermann, and T. P. Martin, *Z. Phys. D* **31**, 191 (1994).

⁵C. Bréchnignac, Ph. Cahuzac, F. Carlier, and M. de Frutos, *Phys. Rev. Lett.* **64**, 2893 (1990); **49**, 2825 (1994).

⁶C. Bréchnignac, Ph. Cahuzac, F. Carlier, J. Leygnier, and A. Sarfati, *Phys. Rev. B* **44**, 11 386 (1991).

⁷C. Bréchnignac, in *Clusters of Atoms and Molecules* (Ref. 1), Vol. I, p. 255.

⁸E. Lipparini and A. Vitturi, *Z. Phys. D* **14**, 57 (1990).

⁹W. A. Saunders, *Phys. Rev. Lett.* **64**, 3046 (1990); **66**, 840 (1991).

¹⁰F. Chandezon, C. Guet, B. A. Huber, D. Jalabert, M. Maurel, E. Monnard, C. Ristori, and C. Rocco, *Phys. Rev. Lett.* **74**, 3784 (1995).

¹¹M. Nakamura, Y. Ishii, A. Tamura, and S. Sugano, *Phys. Rev. A* **42**, 2267 (1990).

¹²H. Koizumi, S. Sugano, and Y. Ishii, *Z. Phys. D* **26**, 264 (1993).

¹³F. Garcias, J. A. Alonso, J. M. López, and M. Barranco, *Phys. Rev. B* **43**, 9459 (1991).

¹⁴F. Garcias, A. Mañanes, J. M. López, J. A. Alonso, and M. Barranco, *Phys. Rev. B* **51**, 1897 (1995).

¹⁵B. K. Rao, P. Jena, M. Manninen, and R. M. Nieminen, *Phys. Rev. Lett.* **58**, 1188 (1987).

¹⁶E. Blaisten-Barojas, Y. Li, and A. Belenki, in *Dynamics in Small*

Confining Systems II, edited by J. M. Drake, J. Klafter, R. Kopelman, and S. M. Trolan, MRS Symposia Proceedings No. 366 (Materials Research Society, Pittsburgh, 1995), p. 341.

¹⁷N. Bohr and J. A. Wheeler, *Phys. Rev.* **56**, 426 (1939).

¹⁸S. N. Khanna, F. Reuss, and J. Buttet, *Phys. Rev. Lett.* **61**, 535 (1988).

¹⁹R. N. Barnett, U. Landman, and G. Rajagopal, *Phys. Rev. Lett.* **67**, 3058 (1991).

²⁰P. Jena, S. N. Khanna, and C. Yannouleas, *Phys. Rev. Lett.* **69**, 1471 (1992).

²¹S. M. Foiles, M. I. Baskes, and M. S. Daw, *Phys. Rev. B* **33**, 7983 (1986).

²²E. Blaisten-Barojas and S. N. Khanna, *Phys. Rev. Lett.* **61**, 1477 (1988).

²³Y. Li, E. Blaisten-Barojas, and D. A. Papaconstantopoulos, *Chem. Phys. Lett.* **268**, 331 (1997).

²⁴W. Zhong, Y. S. Li, and D. Tomanek, *Phys. Rev. B* **44**, 13 053 (1991).

²⁵M. Sigalas and D. A. Papaconstantopoulos, *Phys. Rev. B* **49**, 1574 (1994).

²⁶M. Sigalas, N. C. Bacalis, D. A. Papaconstantopoulos, and A. C. Switendick, *Phys. Rev. B* **42**, 11 637 (1990).

²⁷J. F. Janak, *Phys. Rev. B* **9**, 3985 (1974).

²⁸L. Hedin and B. I. Lundqvist, *J. Phys. C* **4**, 2064 (1971).

²⁹N. W. Ashcroft and N. D. Mermin, *Solid State Physics* (Holt, Rinehart and Winston, New York, 1976).

³⁰C. Fiolhais, J. P. Perdew, S. Q. Armster, James M. Maclaren, and M. Brajczewska, *Phys. Rev. B* **51**, 14 001 (1995).

³¹M. S. Anderson and C. A. Swenson, *Phys. Rev. B* **28**, 5395 (1983).

³²D. A. Papaconstantopoulos, *Handbook of the Band Structure of*

- Elemental Solids* (Plenum, New York, 1986).
- ³³G. C. Kallinteris, N. I. Papanicolaou, G. A. Evangelakis, and D. A. Papaconstantopoulos, *Phys. Rev. B* **55**, 2150 (1997).
- ³⁴R. Poteau, D. Maynaud, J. P. Daudey, and F. Spiegelmann, *Z. Phys. D* **26**, 232 (1993).
- ³⁵F. A. Lindemann, *Z. Phys.* **11**, 609 (1910).
- ³⁶*Handbook of Chemistry and Physics*, edited by D. R. Lide, 73rd ed. (CRC, Boca Raton, FL, 1993).
- ³⁷G. Ernst, *Acta Phys. Austriaca* **33**, 27 (1971).
- ³⁸H. Ibach and H. Lüth, *Solid State Physics* (Springer, New York, 1995).
- ³⁹T. P. Martin, T. Bergmann, H. Göhlich, and T. Lange, *J. Phys. Chem.* **95**, 6421 (1991).
- ⁴⁰W. D. Knight, K. Clemenger, W. A. de Heer, W. A. Sauders, M. Y. Chou, and M. L. Cohen, *Phys. Rev. Lett.* **52**, 2141 (1984).
- ⁴¹H. Göhlich, T. Lange, T. Bergmann, and T. P. Martin, *Phys. Rev. Lett.* **65**, 748 (1990).
- ⁴²C. Bréchnignac, Ph. Cahuzac, F. Carlier, M. de Frutos, and J. Roux, *Phys. Rev. B* **47**, 2271 (1993).
- ⁴³F. Chandezon, P. M. Hansen, C. Ristori, J. Pedersen, J. Westergaard, and S. Bjornholm, *Chem. Phys. Lett.* **277**, 450 (1997).
- ⁴⁴N. D. Bhaskar, R. P. Fueholz, C. M. Klimcak, and R. A. Cook, *Phys. Rev. B* **36**, 4418 (1987).
- ⁴⁵T. Bergmann, H. Göhlich, T. Lange, T. Bergmann, and T. P. Martin, *Phys. Rev. Lett.* **65**, 748 (1990).
- ⁴⁶V. M. Strutinsky, *Nucl. Phys. A* **122**, 1 (1968); see also, M. Brack, *Rev. Mod. Phys.* **65**, 677 (1993).
- ⁴⁷V. Bonačić-Koutecký, P. Fantucci, and J. Koutecký, *Phys. Rev. B* **37**, 4369 (1988).
- ⁴⁸U. Röthlisberger and W. Andreoni, *J. Chem. Phys.* **94**, 8129 (1991).
- ⁴⁹T. P. Martin, *Phys. Rep.* **273**, 199 (1996).
- ⁵⁰E. Blaisten-Barojas and D. Levesque, *Phys. Rev. B* **34**, 3910 (1986).
- ⁵¹J. L. Martins, J. Buttet, and R. Car, *Phys. Rev. B* **31**, 1804 (1985).
- ⁵²K. M. Kanal, A. K. Ray, and I. A. Howard, *Phys. Status Solidi B* **171**, 131 (1992).
- ⁵³Y. Li, Doctoral thesis, George Mason University, July, 1997.
- ⁵⁴M. R. Zachariah, M. Carrier, and E. Blaisten-Barojas, *J. Phys. Chem.* **100**, 14 856 (1996).
- ⁵⁵M. J. Mehl and D. A. Papaconstantopoulos, *Phys. Rev. B* **54**, 4519 (1996).
- ⁵⁶Lord Rayleigh, *Philos. Mag.* **14**, 185 (1882).